Three–Dimensional Computations of Time–Dependent Incompressible Flows with an Implicit Multigrid–Driven Algorithm on Parallel Computers

Andrey Belov, Luigi Martinelli and Antony Jameson,
Department of Mechanical and Aerospace Engineering, Princeton University,
Princeton N.J. 08544, U.S.A. (609) 258-3749, belov@cougarxp.princeton.edu

The present work is aimed at the development of a robust, computationally efficient algorithm for the simulation of unsteady incompressible flows of interest in engineering. In particular, we focus on the extension of a fully-implicit multigrid driven algorithm, originally proposed and validated for both the two-dimensional Euler and Navier-Stokes equations in references [1,2], to three dimensions.

The vortex shedding from a circular cylinder has been recently investigated by a number of authors with the focus on the mechanism of momentum and vorticity transport [4, 5] and on the active control of the wake structure [6]. The transition of the flow to a three-dimensional mode ($180 \leq Re \leq 260$) attracts particular interest. In this regime the slow asymptotics of the wake provides a challenging test for numerical methods since long integration times are necessary to resolve the flow evolution toward a limiting cycle. In the present work, time-resolved computations of vortex shedding from a circular cylinder for Reynolds numbers between 45 and 250 are performed to assess both accuracy and parallel efficiency of the present algorithm. The vortex wake structure as well as the averaged flow quantities for this flow regime are found to be in a good agreement with the experimental and computational data, obtained by other authors.

Computational Algorithm

The governing equations of the flow considered are the nonlinear time-dependent incompressible Navier-Stokes equations of a laminar, constant viscosity flow without body forces. Spatial residuals are discretized using a cell-centered finite volume approach. Our method, presented in references [1, 2, 15], couples Chorin's artificial compressibility approach [7] with an inner iteration to solve an implicit backward discretization of the unsteady terms of order two or higher. As was proposed by Jameson for time accurate compressible flow computations [9], the resulting pseudotransient problem is solved by the highly efficient multigrid time stepping technique originally developed by Jameson[3] for compressible flow calculations. The solution of the pseudotransient problem at each time step provides a direct coupling between the velocity and pressure fields, and satisfies the divergence-free constraint, as in the scheme of Kwak et al [10]. Similar strategy has been employed by Taylor and Whitfield [11] by coupling the Newton's iteration with an upwind flux-difference splitting scheme. Miyake et al. [12] used an explicit, up to a second order accurate discretization in time, and a rational Runge-Kutta scheme for the subiterations. In the present work the temporal derivatives are treated in a point-implicit fashion, following [13], to uncouple the pseudotime step from the physical time step and improve computational efficiency of the algorithm even further. The flow solver is implemented in parallel by using Message Passing Interface (MPI) Standard on a multiprocessor IBM SP2 computer.

For viscous calculations, a no-slip condition is imposed on the solid boundary by setting the flow velocity equal to that of the body. Since the present work addresses the low Reynolds

number regime ($Re \leq 250$) the pressure gradient is not assumed to be zero, it is derived from a balance with the normal components of the viscous stress and body acceleration. Accordingly, a second order accurate central difference discretization of the $\frac{dP}{dn}$ at the solid boundary is used to compute an approximation for the pressure. Note that in the parallel implementation this boundary condition has a higher computational cost as compared to the zero pressure gradient approximation - an extra message with the velocity component updates has to be exchanged by the processors in order to compute the viscous stress tensor.

Periodic spanwise boundary conditions are employed in the present work to simulate a body of an infinite span. On the outer boundaries, approximate non-reflecting far-field boundary conditions are constructed from the linearized characteristics to improve accuracy and the rate of convergence in pseudotime. The linearized characteristic problem is solved along the direction normal to the boundary of the computational domain for P, u_1 and u_2, each time the flow variables are being updated [2]. In the current implementation, the spanwise velocity component u_3 is treated as a passive scalar, and is either extrapolated from the interior of the computational domain or is taken to be equal to its free stream value, depending on the local flow direction. A better approximation to the characteristic far-field boundary conditions can be constructed using the full three-dimensional similarity transform, proposed in reference [14], and it will be implemented in future work.

Results and Discussion

The unsteady laminar vortex shedding from a circular cylinder for $Re \leq 250$, based on the cylinder diameter and a free stream velocity, was selected as a test problem. Experimental studies of the wake of circular cylinders [16, 17] showed that a parallel shedding can be observed in the range of $49 < Re < 180$, provided that special care is taken to control the end effects. Above $Re = 180$, three-dimensional shedding modes are observed, while for $Re < 49$ the wake is stationary. A continuous relation $St(Re)$ of the form

$$St(Re) = \frac{A}{Re} + B + C \cdot Re, \tag{1}$$

where A, B and C are constants, was proposed by Williamson [17] to describe the parallel vortex shedding, believed to be accurate within 1 %. Also, as originally proposed by G.Brown and shown in [17], the experimental data for the three-dimensional oblique shedding in the same range of Re numbers do collapse on the same "universal curve" 1, provided that the Strouhal number is scaled with the inverse cosine of the shedding angle. These findings suggest that a comparison of numerical results with the empirical relation 1 provides a particularly meaningful validation of any numerical method. Such a study has been recently carried out by R.Henderson [19] using an unstructured spectral element method.

The experimental $St(Re)$ data of Williamson [17] are shown in Figure 4 for the range $49 < Re < 250$ by a solid line with the ticks indicating an estimated accuracy of $\pm 1\%$. The corresponding variation of the base pressure coefficient $Cpb(Re)$ is shown in Figure 5 with the ticks illustrating $\pm 2\%$ deviation. A number of other experimental and computational results [17, 19, 18, 20] is also presented in Figure 4. The curve fitting coefficients corresponding to Equation 1 can be found in reference [2].

According to the results of a mesh refinement and domain truncation study [2], a two-dimensional 128×128 O-mesh with the far field boundary placed at a distance of 16 diameters

from the center of the cylinder provides a suitable compromise between accuracy – within a fraction of a percent – and cost of the computation. The parallel implementation of our computational algorithm enabled the complete universal $St(Re)$ curve to be sampled within less than 10 hours using 8 processors of the IBM SP-2 computer. Between 900 and 2000 time steps with $dt = .125$ were computed to ensure that the asymptotic shedding cycle is reached. Once the asymmetric shedding developed, 15 multigrid W-cycles per time step (with six grid levels) were sufficient to enforce the divergence free constraint in each cell better than 10^{-4}, as measured by the maximum continuity residual and better than 2×10^{-6} in the root mean squared residual. In order to speed up the transition to a limiting cycle, the cylinder was initially rotated about it's center with the amplitude of 2° and then stopped. The initial motion with different amplitudes seem to influence the onset time of the asymmetric shedding, but not the characteristics of the limiting cycle itself.

The computed data are shown in Figure 4 by stars and found to be in excellent – better than 1%– agreement with the "universal curve" in the range of Reynolds numbers $50 \leq Re \leq 200$. Our data are also in good agreement with the experimental curve obtained by Roshko [18] and the spectral element computations by Henderson [19]. The variation of the base pressure coefficient with Reynolds number $Cpb(Re)$ is shown in Figure 5. Our data exhibit the same trend as other computational and experimental results [19, 18] and lie within the experimental errors quoted at $1\% \div 5\%$.

Below $Re < 49$, the wake of a circular cylinder is stationary [16]. Our calculations with $Re = 50$ and $Re = 60$ required considerably more time steps to develop the shedding then the computations with higher Reynolds numbers. In the case with $Re = 45$ a decaying response was observed. These results further confirm that the present method captures correct asymptotic behavior of the wake flows within the considered range of Reynolds numbers.

The two-dimensional computations for Reynolds numbers above 180 fail to capture the transition of the flow to a three-dimensional mode and consequently deviate from the experimental data, Figure 4. Three-dimensional computations were performed on a $96 \times 64 \times 32$ O-H-mesh for a cylinder with an aspect ratio $L/D = 6.4$. An initial disturbance is introduced in the flow to expedite the onset of the shedding. The disturbance imitates a distributed torsional deformation of a cylinder: spanwise sections of a cylinder are rotated in their planes with the common frequency but with the random number generated amplitude between 0° and 5° degrees and then stopped. Spanwise variation of the base pressure coefficient $d(Cpb) = Cpb_{max} - Cpb_{min}$ is considered as one of the indicators of the flow three-dimensionality. It's time history is shown in Figure 1 for $Re = 150$ and $Re = 225$. The results for $Re = 150$ exhibit a decaying response to the initial disturbance and reach, asymptotically, a two-dimensional shedding, which is in agreement with the experimental predictions. At $Re = 225$ the flow is unstable to the same disturbance: initially the flow develops essentially two-dimensional shedding, and then, the $d(Cpb)$ and the maximum spanwise velocity component gradually increase by two orders in magnitude until the fully evolved 3-D shedding. The time-averaged flow quantities corresponding to the initial parallel shedding regime agree reasonably well with those computed by the two-dimensional solver, as compared in Table 1, given the difference in spatial resolution of the two meshes. The time evolution of the lift coefficient for the $Re = 225$ case is shown in Figure 2. The onset of the three-dimensionality is marked by a sharp reduction in the lift coefficient, the Strouhal frequency and the base suction $(-Cpb)$. This is similar to the results of a computation with $Re = 525$, described

Quantity	2-D Solver, Grid 128x128	3-D Solver, Grid 96x64x32	
	2-D Shedding	Initial 2-D Shedding	3-D Shedding
Cl	±0.703	±0.701	Modulated
Cdmax	1.26	1.27	1.20
Cpb	-1.00	-1.02	-0.855
St	0.201	0.205	0.186

Table 1: **Comparison of the 2-D and 3-D results, Re=225.**

in reference [4]. Modulation of the lift coefficient was observed for the fully developed flow regime, presumably indicating the formation of vortices with varying degrees of coherence along the spanwise direction. One can observe the two distinctive patterns in time histories of $d(Cpb)$ and the Cl, superimposed in Figure 3. The "coherent" ("C") regime possesses the highest lift amplitude and corresponds to the lower values of $d(Cpb)$, which seems to indicate that the flow in the nearest vicinity of the cylinder is virtually two-dimensional. The highly irregular, large amplitude excursions in $d(Cpb)$ are visible in "uncorrelated" ("U") regime, suggesting that not only the wake but also the vortex formation region right next to the surface of a cylinder are highly three-dimensional. These considerations might indicate that the regime where transition to three-dimensionality occurs migrates up- and downstream between the cylinder and the near wake, giving rise to the modulation of the Cl.

Time-averaged results for the three-dimensional shedding mode for Reynolds numbers 250 and 225 are shown in Figures 4 and 5 with circles. The fully developed flow regime was resolved using 40 time steps per shedding cycle with 25 five-level W-multigrid cycles per time step. This required less than 3 min. per time step using 6 wide nodes (RS6000/590) of IBM SP2. The parallel speedup achieved by our algorithm is presented in Figure 8. Excellent agreement is observed with the lower branches of the experimental data curves corresponding to the shedding mode "A" as defined in reference [17]. According to this source, the "A" mode of vortex shedding is characterized by the presence of the streamwise vortex loops with a spanwise wavelength of about 3 diameters. Figures 6, 7 show that similar structures are observed in our computation with the wavelength equal to 3.2 diameters. The ***bulges*** and ***valleys***, observed in our computation, appear to be similar to the vortical structures widely described in literature.

Further analysis of the flow regime using a finer mesh and higher aspect ratio cylinder is necessary to establish grid independence and to investigate the vorticity transport mechanism in more detail. This work will be presented at future meetings.

Conclusions

A computational algorithm which couples the artificial compressibility approach with a very efficient multigrid acceleration technique has been extended to three dimensions.

Analysis of the test calculations performed so far indicates that our time-accurate solver is very efficient for applications in the unsteady incompressible flow regime. The results presented above compare favorably with available experimental data and with numerical results computed by other authors. We conclude that the proposed scheme provides an accurate and efficient way of computing time-dependent incompressible flows. This suggests

that the time-resolved computations over the geometries of engineering complexity can be obtained in less than one hour per convective time-scale. For example, this could be a computation of the maneuver of a full configuration submarine or a yacht.

Acknowledgement

We are grateful to Dr. Henderson for providing us with his data. Support for this work was provided through by the Office of Naval Research through Grant N00014-93-I-0079, under the supervision of Dr. E.P. Rood.

References

[1] Belov, A., Martinelli, L., Jameson, A.: 2nd European CFD Conf., Germany (1994)
[2] Belov, A., Martinelli, L., Jameson, A.: AIAA Paper 95-0049 (1995)
[3] Jameson, A.: Appl. Math. & Comput., Vol.13, pp.327-356 (1983)
[4] Balachandar, S., Mittal R.: 10th Symp. on Turbulent Shear Flows (1995)
[5] Prasad, A.,Williamson, C.H.K.: 10th Symp. on Turbulent Shear Flows (1995)
[6] Persillon, H., Braza, M., HaMinh, H. Williamson, C.H.K.: 10th Symp. on T.S.F. (1995)
[7] Chorin, A.J.: J. of Comp. Phys., Vol. 2, pp. 12-26 (1967)
[8] Rizzi, A., Eriksson L.-E.: J. of Fluid Mech., Vol. 153, pp. 275-312 (1985)
[9] Jameson, A.: AIAA Paper 91-1596 (1991)
[10] Rogers, S.E., Kwak, D.: AIAA J., Vol. 28, No. 2, pp. 253-262 (1990)
[11] Taylor, L.K., Whitfield, D.L.: AIAA Paper 91-1650 (1991)
[12] Miyake, T., Sakamoto, Y., Tokunaga, H., Satofuka, N.: 1st European CFD Conf. (1992)
[13] Melson, N., Sanetrik, M., Atkins, H.: 6th Copper Mount. Conf. on Multig. Meth. (1993)
[14] Rogers, S.E., Chang, J.L.C., Kwak, D.: J. of Comp. Phys., Vol. 73, No. 2 (1987)
[15] Belov, A., Martinelli, L., Jameson, A.: 6th International Symp. on CFD (1995)
[16] Williamson, C.H.K., Roshko, A.: Z.Flugwiss. Weltraumforsch, 14, pp.38-46 (1990)
[17] Williamson, C.H.K.: Phys. Fluids, Vol. 31, pp. 2742-2744 (1988)
[18] Roshko, A.: NACA Rep.1191 (1954)
[19] Henderson, R.D.: Ph.D. Thesis, MAE Dept., Princeton University (1994)
[20] Henderson, R.D., Private communication.

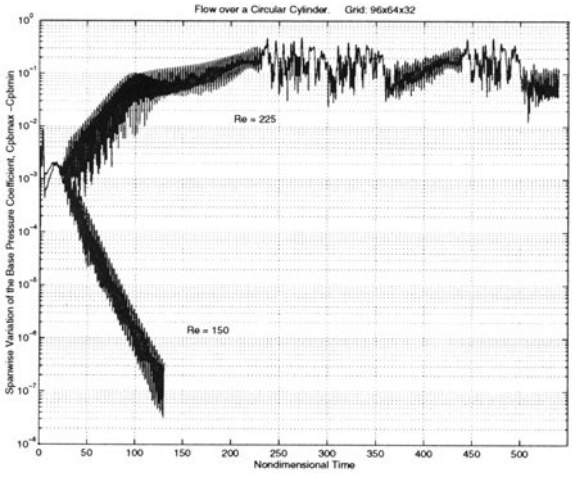

Figure 1: Time History of the Spanwise Variation of Cpb, Re=150 and Re=225.

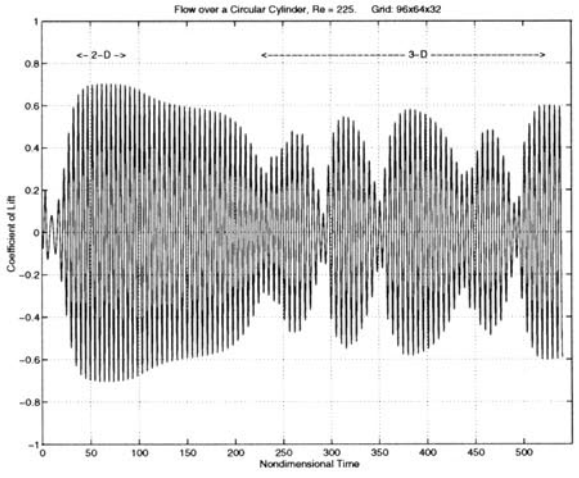

Figure 2: Evolution of the Lift Coefficient.

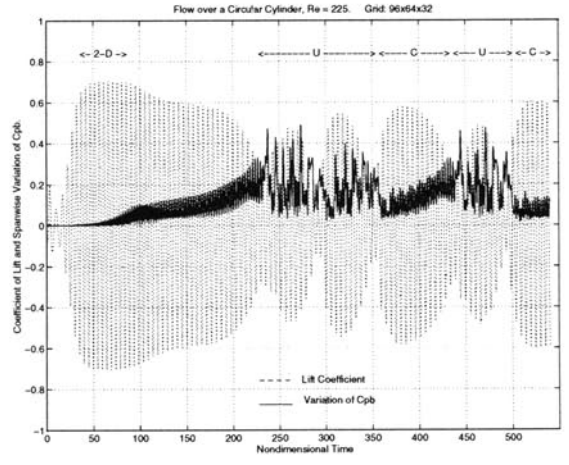

Figure 3: Evolution of Cl and d(Cpb).

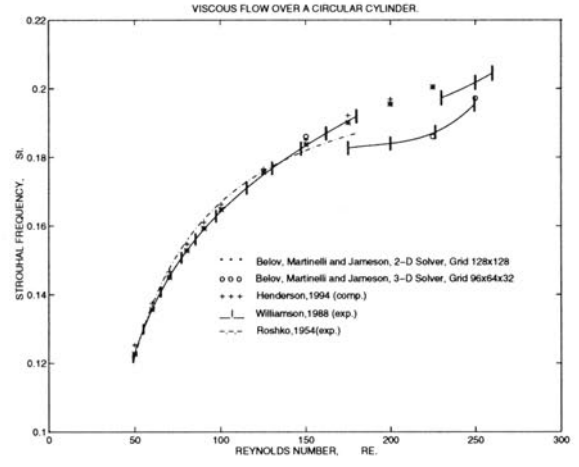

Figure 4: The Strouhal Frequency, St(Re).

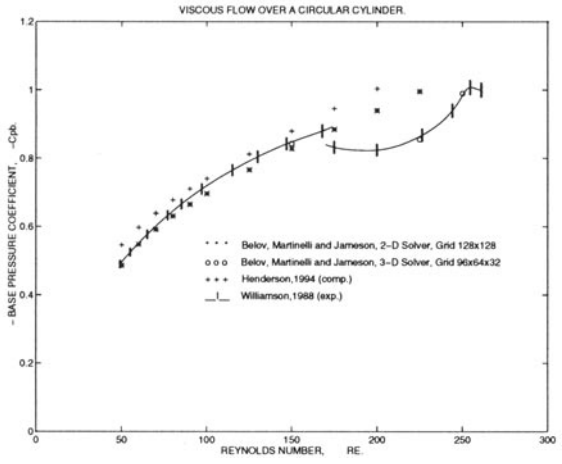

Figure 5: The Base Pressure Coefficient.

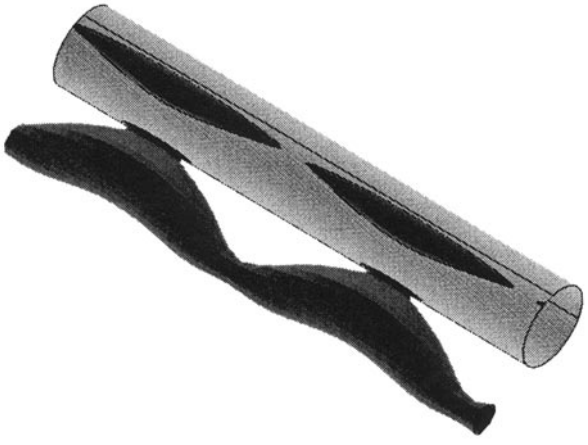

Figure 6: Isosurface of Pressure, Re=250.

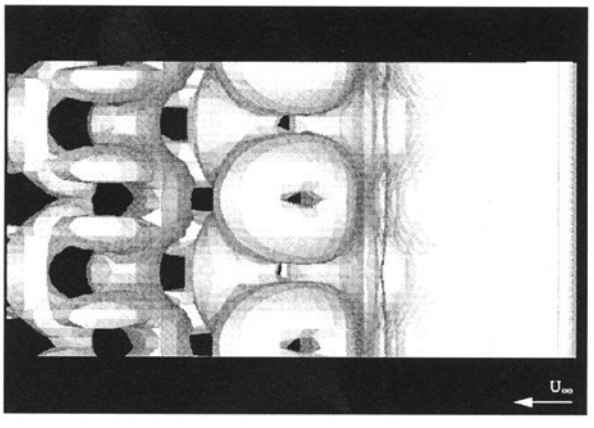

Figure 7: Vorticity, Re=250 (Top View).

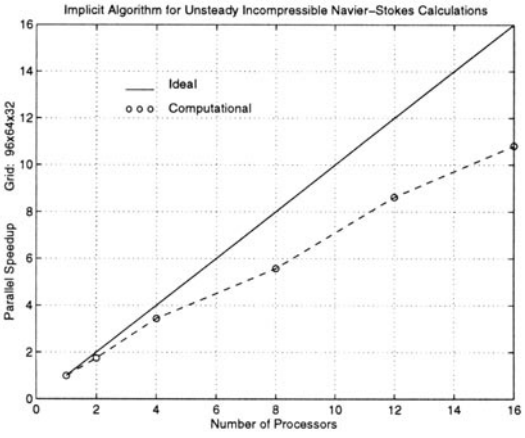

Figure 8: Parallel Speedup.